



PHYSICA



NONLINEAR PHENOMENA

Coordinating Editors:

C.K.R.T. JONES (Editor-in-Chief)
A. DOELMAN (Distributing Editor)
J. LEGA (Special Issues Editor)

Editors

R.P. BEHRINGER	J. PEARSON
M. BRENNER	A. PIKOVSKY
J. BRONSKI	K. PROMISLOW
S. COOMBES	V. ROM-KEDAR
H. DIJKSTRA	R. ROY
J. GARNIER	B. SANDSTEDE
S. KAI	T. SAUER
H. LEVINE	M. SILBER
D. LOHSE	J. STARK
I. MEZIC	G. STEPAN
A.S. MIKHAILOV	R. TEMAM
A.C. NEWELL	M. VERGASSOLA
Y. NISHIURA	

***last issue
of this volume***

Available online at

 **ScienceDirect**
www.sciencedirect.com

<http://www.elsevier.com/locate/physd>

This article was published in an Elsevier journal. The attached copy is furnished to the author for non-commercial research and education use, including for instruction at the author's institution, sharing with colleagues and providing to institution administration.

Other uses, including reproduction and distribution, or selling or licensing copies, or posting to personal, institutional or third party websites are prohibited.

In most cases authors are permitted to post their version of the article (e.g. in Word or Tex form) to their personal website or institutional repository. Authors requiring further information regarding Elsevier's archiving and manuscript policies are encouraged to visit:

<http://www.elsevier.com/copyright>



The effects of unequal diffusion coefficients on periodic travelling waves in oscillatory reaction–diffusion systems

Matthew J. Smith*, Jonathan A. Sherratt

Department of Mathematics and the Maxwell Institute for Mathematical Sciences, Heriot-Watt University, Edinburgh, EH14 4AS, UK

Received 18 April 2006; received in revised form 21 July 2007; accepted 25 July 2007

Available online 29 July 2007

Communicated by B. Sandstede

Abstract

Many oscillatory biological systems show periodic travelling waves. These are often modelled using coupled reaction–diffusion equations. However, the effects of different movement rates (diffusion coefficients) of the interacting components on the predictions of these equations are largely unknown. Here we investigate the ways in which varying the diffusion coefficients in such equations alters the wave speed, time period, wavelength, amplitude and stability of periodic wave solutions. We focus on two sets of kinetics that are commonly used in ecological applications: lambda–omega equations, which are the normal form of an oscillatory coupled reaction–diffusion system close to a supercritical Hopf bifurcation, and a standard predator–prey model. Our results show that changing the ratio of the diffusion coefficients can significantly alter the shape of the one-parameter family of periodic travelling wave solutions. The position of the boundary between stable and unstable waves also depends on the ratio of the diffusion coefficients: in all cases, stability changes through an Eckhaus (‘sideband’) instability. These effects are always symmetrical in the two diffusion coefficients for the lambda–omega equations, but are asymmetric in the predator–prey equations, especially when the limit cycle of the kinetics is of large amplitude. In particular, there are two separate regions of stable waves in the travelling wave family for some parameter values in the predator–prey scenario. Our results also show the existence of a one-parameter family of travelling waves, but not necessarily a Hopf bifurcation, for all values of the diffusion coefficients. Simulations of the full partial differential equations reveals that varying the ratio of the diffusion coefficients can significantly change the properties of periodic travelling waves that arise from particular wave generation mechanisms, and our analysis of the travelling wave families assists in the understanding of these effects.

© 2007 Elsevier B.V. All rights reserved.

Keywords: AUTO; Essential spectrum; Wave train; Numerical continuation

1. Introduction

The components of many biological systems exhibit regular temporal cycles. These are sometimes an emergent property from the interactions between different components of the system. Periodic waves also occur in a wide variety of biological systems, ranging from intracellular chemodynamics such as calcium signalling, to cyclic population dynamics in ecology [2–8]. A natural hypothesis is that these waves arise from the combination of oscillatory local dynamics and diffusive-type dispersal (reviewed in [1]).

Reaction–diffusion models are traditionally used to study systems exhibiting periodic travelling waves (see Fig. 1(c), for example dynamics). These combine diffusion in space with reaction kinetics that are intrinsically oscillatory in time. The standard mathematical form for reaction–diffusion models with two interacting (and oscillating) components is

$$\frac{\partial u}{\partial t} = D_u \frac{\partial^2 u}{\partial x^2} + f(u, v) \quad (1a)$$

$$\frac{\partial v}{\partial t} = D_v \frac{\partial^2 v}{\partial x^2} + g(u, v) \quad (1b)$$

where $u(x, t)$ and $v(x, t)$ are the quantities (e.g. animal population sizes) of the interacting components of the system,

* Corresponding author. Tel.: +44 0 131 451 3253; fax: +44 0 131 451 3249.
E-mail address: m.j.smith@ma.hw.ac.uk (M.J. Smith).

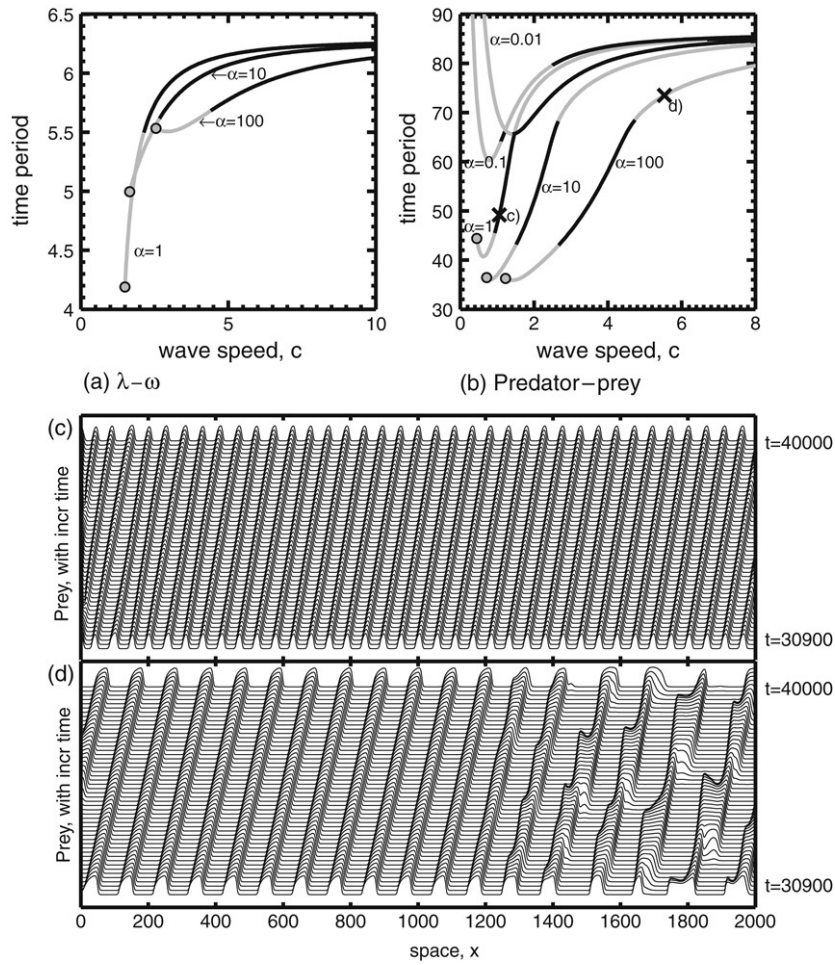


Fig. 1. Comparison of the effects of varying α on the wave family predicted by travelling wave equations (8) with reaction kinetics of λ - ω form ((a)—Eqs. (3) and (4), with $\omega_0 = 1.5$ and $\omega_1 = 0.5$) or predator–prey form ((b)—Eqs. (9), with $\sigma = 0.15$, $\mu = 0.05$ and $\kappa = 0.2$). Grey-filled circles indicate the position of c_{Hopf} from which the wave family emanates (Eqs. (12) and (13)). c_{Hopf} doesn't exist for lines with no filled circles. Grey lines denote unstable waves and black lines denote stable waves. Note that in (b) stability changes at $c = 6.7$ when $\alpha = 1$. Stability also changes at $c = 18.0$ and $c = 34.8$ when $\alpha = 10$ and $\alpha = 100$, respectively (not shown). See (Section 2) for details on the calculation of wave families and their stability. The labelled crosses denote periodic travelling waves selected in simulations of Eqs. (1) that are illustrated in (c) and (d). In (c) and (d), Eq. (1) were solved numerically as detailed in Section 5. The zero Dirichlet boundary conditions are at $x = 0$ and the zero Neumann boundary conditions are at $x = 2000$.

x and t denote space and time, respectively, and the diffusion coefficients D_u and D_v are positive constants. The functions f and g will be of a form giving a stable limit cycle solution in the kinetic ordinary differential equations.

For systems exhibiting periodic travelling waves, the appropriate solution forms are $u(x, t) = U(z)$ and $v(x, t) = V(z)$, where $z = (x/c) - t$ is the travelling wave coordinate and c is the wave speed. Substituting these into Eqs. (1) gives

$$(D_u/c^2)U'' + U' + f(U, V) = 0, \quad (2a)$$

$$(D_v/c^2)V'' + V' + g(U, V) = 0, \quad (2b)$$

where prime denotes d/dz . Periodic travelling wave solutions of reaction–diffusion equations were first studied by Kopell and Howard [9]. They showed that, provided D_u and D_v are sufficiently close, a system of equations of the form (2) has a one-parameter family of limit cycle solutions, corresponding to periodic travelling waves. They studied in detail the case of

$D_u = D_v$, with f and g having “ λ - ω ” form

$$f(u, v) = \lambda(r)u - \omega(r)v, \quad (3a)$$

$$g(u, v) = \omega(r)u + \lambda(r)v, \quad (3b)$$

where $r = (u^2 + v^2)^{1/2}$. This remains the prototype system for oscillatory reaction–diffusion systems, and natural specific forms for λ and ω are

$$\lambda(r) = 1 - r^2, \quad (4a)$$

$$\omega(r) = \omega_0 - \omega_1 r^2, \quad (4b)$$

where for simplicity we assume that the constants ω_0 and ω_1 satisfy $\omega_0 > \omega_1 > 0$. One advantage of studying travelling wave equations with reaction kinetics formulated in this way is that the family of periodic waves then has a very simple analytical form, namely

$$u = \hat{r} \cos[\omega(\hat{r})t \pm \lambda(\hat{r})^{1/2}x] \quad (5a)$$

$$v = \hat{r} \sin[\omega(\hat{r})t \pm \lambda(\hat{r})^{1/2}x] \quad (5b)$$

where $\hat{r} \in (0, 1)$ parametrises the wave family [9]. As wave amplitude, \hat{r} , increases from 0 to 1, the spatial wavelength $2\pi/\lambda(\hat{r})^{1/2}$ increases from 2π to infinity, the time period $2\pi/\omega(\hat{r})$ increases from $2\pi/\omega_0$ to $2\pi/(\omega_0 - \omega_1)$ and the wave speed $\omega(\hat{r})/\lambda(\hat{r})^{1/2}$ increases from ω_0 to infinity. Note that in the case $D_u = D_v$ and $\omega_0 = 0$, Eqs. (2) becomes the complex Ginzburg–Landau equation with zero linear dispersion (see for example [41], Sec. II.B).

Kopell and Howard [9] showed that the stability of the travelling waves as solutions of Eqs. (1) and (3) on unbounded domains, also changes along the one-parameter family, with the exact condition for stability being

$$4\lambda(\hat{r}) \left[1 + \left(\frac{\omega'(\hat{r})}{\lambda'(\hat{r})} \right)^2 \right] - \lambda'(\hat{r}) \leq 0. \quad (6)$$

This implies that sufficiently low amplitude waves are always unstable and sufficiently high amplitude waves are always stable. Here, and throughout this paper, we are referring to wave stability on unbounded domains.

The analytical tractability of Eqs. (3) and (4), when $D_u = D_v$, has led to their use in studies of periodic travelling waves in oscillatory biological systems [1,15,30]. The case of $D_u \approx D_v$ can be studied using perturbation theory (see [10]), but to study the waves more generally, we use numerical bifurcation software (see Section 2 for details). Plotting the time period against the wave speed is a standard way of presenting the wave family. In Fig. 1, for example, we illustrate the wave family for kinetics of λ – ω form, and also for kinetics that are a standard model for cyclic populations in ecology [31,32]. The figure demonstrates that changing the diffusion coefficients alters both the shape of the wave family, and the way in which wave stability varies along it, for both sets of kinetics. The properties of travelling waves commonly measured in ecological studies are the amplitude (e.g. in numbers of individuals), speed (e.g. in kilometres per year), wavelength (e.g. in kilometres), and time period (in years), and so we focus on these measures in this study. However, the latter two are straightforward functions of wave number ($2\pi/\text{wavelength}$) and frequency ($2\pi/\text{time period}$), that are more commonly used in physics.

In ecological systems, the diffusion coefficients of the two (or more) components in oscillatory reaction–diffusion equations are likely to be different. Therefore, it is an important question to ask how the properties of the wave family are affected by such differences. A partial answer to this question is revealed by rewriting Eqs. (2) with $\alpha = D_u/D_v$ and $\beta = D_u D_v$ to give

$$(\sqrt{\alpha\beta}/c^2)U'' + U' + f(U, V) = 0, \quad (7a)$$

$$(\sqrt{\beta}/\sqrt{\alpha}c^2)V'' + V' + g(U, V) = 0. \quad (7b)$$

This shows that the product of the diffusion coefficients β simply scales the travelling wave speed. Eqs. (2) can therefore be simplified further by using a rescaled wave speed $c^* = c/\beta^{1/4}$ to give (dropping ‘*’s)

$$(\sqrt{\alpha}/c^2)U'' + U' + f(U, V) = 0, \quad (8a)$$

$$(1/c^2\sqrt{\alpha})V'' + V' + g(U, V) = 0. \quad (8b)$$

A less simple question to answer, however, is how the wave properties are affected by the ratio of the diffusion coefficients (α). In this paper we give results that provide a partial answer to this question. We firstly investigate how variation in α affects the wave speed at the Hopf bifurcation of the wave family (filled circles in Fig. 1(a) and (b)). Next, we explore numerically how varying α affects the shape of the family of travelling wave solutions (lines in Fig. 1(a) and (b)), and the location of stable/unstable regions (black/grey lines in Fig. 1(a) and (b)). Finally, we use numerical simulations of the partial differential equations (1) to explore how varying α affects the particular member of the travelling wave family generated by two important classes of initial condition (e.g. crosses in Fig. 1(b)–(d)).

In these various studies, we focus on two sets of reaction kinetics used commonly in studies of periodic travelling waves in ecology [15,21,30]: the λ – ω system given in (3), and a standard model for cyclic predator–prey dynamics [31,32]. The λ – ω reaction kinetics (Eqs. (3) and (4)) are the normal form of any coupled oscillatory system close to a supercritical Hopf bifurcation. Therefore, any such system can be approximated by the λ – ω equations using the standard mathematical theory of normal forms. Studying the λ – ω equations is thus of general relevance to oscillatory reaction–diffusion equations. The predator–prey kinetic equations are

$$f(u, v) = u(1 - u) - \frac{uv}{u + \kappa}, \quad \text{and} \quad (9a)$$

$$g(u, v) = \frac{\sigma uv}{u + \kappa} - \mu v, \quad (9b)$$

where u and v are the densities of prey and predators, respectively, μ is the predator death rate, σ is the predator–prey conversion rate, and κ is the half-saturation constant in the hyperbolic functional response. Eqs. (9) have been re-scaled such that $0 < u < 1$ and have non-trivial steady state solutions $u_s = \mu\kappa/(\sigma - \mu)$ and $v_s = (1 - u_s)(u_s + \kappa)$. Throughout this paper we fix $\sigma = 0.15$ and $\mu = 0.05$, and study the effects of varying κ . We also assume that $0 < \kappa < 0.5$, since in this region u_s and v_s are locally unstable and the kinetics have a stable limit cycle. Sufficiently far from the Hopf bifurcation (at $\kappa = 0.5$), these limit cycles can differ significantly from the sinusoidal oscillations that occur very close to the Hopf bifurcation (and which are always predicted by λ – ω kinetics). Our hypothesis was that because of this, ratios of predator and prey diffusion coefficients above and below 1 would have different effects on the family of travelling waves.

2. Details on numerical computations

We used AUTO bifurcation and continuation software [11–13] to compute the periodic solutions of the travelling wave equations (8) and their stability. We only give a general overview of our approach here since details of our methodology are given in [11–13,33]. Similar methods were used by [33,38,39] for other systems.

For given kinetic equations and parameters, the one-parameter family of periodic travelling waves (such as

in Fig. 1(a) and (b)) can be computed by performing a continuation of the limit cycle solutions of Eqs. (8) as wave speed is increased, starting at the wave speed of the Hopf bifurcation of these equations, c_{Hopf} . In the scenarios where c_{Hopf} doesn't exist we located the wave family by labelling a solution of specified time period in the wave family for $\alpha = 1$ (which can always be found, see [9]) and then performing a continuation in α to locate a solution of the same period but for the required value of α .

The stability of periodic travelling wave solutions can be computed by linearising Eqs. (8) about the wave, and computing the spectrum of the resulting eigenvalue problem. Full details of the approach we used are given in [33], however we give a brief summary of the technique here. We first calculated eigenvalues corresponding to eigenfunctions that are periodic over one wavelength, by discretising in z to give a (large) algebraic eigenvalue problem; we consider only eigenvalues with an appropriately large real part. The spectrum is then computed by continuation of the real and imaginary parts of these eigenvalues as the phase difference in the eigenfunction across one wavelength is increased from 0 to 2π . This is done sequentially, starting at each of the eigenvalues corresponding to periodic eigenfunctions. This gives the essential spectrum of the wave. Waves are stable (on an infinite domain) if and only if their essential spectrum contains only points with negative real part, other than the origin, which is always an eigenvalue and corresponds to a translation of the wave.

Using this technique, we investigated wave stability for a wide range of wave speeds and α values. The transition from stable to unstable waves occurs through an Eckhaus instability [33,34] at the origin in the eigenvalue complex plane in all cases we studied. In contrast, in some other reaction diffusion systems periodic waves can destabilise through a Hopf bifurcation; see Fig. 12(b) in [38], for example. The boundary between stable and unstable waves in the c - α plane can be computed by numerical continuation of this Eckhaus bifurcation point. Again, full details of the approach are given in [33] and we only give a brief summary. We differentiate the eigenvalue equation twice with respect to the phase difference in the eigenfunction over one wavelength. This gives a system of coupled differential equations that includes the second derivative of the real part of the eigenvalue, zeros of which define Eckhaus points. We numerically continue the locations of these zeros to trace the stability/instability boundary for periodic waves. An appropriate starting point for this continuation can be found via sufficiently precise estimation of the wave speed at an Eckhaus point for one value of α , via explicit computation of the essential spectrum. However in the λ - ω case this is unnecessary because an appropriate starting point is $\alpha = 1$ and the critical wave speed given in Eq. (6).

In the stability analysis we focused on the parameter ranges $0.01 \leq \alpha \leq 100$ and $0 \leq c \leq 10$. We also computed the stability of solutions to Eqs. (8), for the different scenarios, when $c = \infty$, which corresponds simply to the limit cycle of the kinetic equations. This spatially synchronous solution is known

to be stable to spatially varying perturbations when $\alpha = 1$, but can be unstable when $\alpha \neq 1$ [9]. When $c = \infty$ Eqs. (8) are functions of U and V with only time dependent coefficients, making stability much easier to calculate than for finite values of c . Solutions can be separated into Fourier modes, and for each Fourier wavenumber, numerical computation of the (two) Floquet exponents is straightforward. This showed that for all parameter sets considered in the remainder of this paper, the spatially homogeneous oscillations corresponding to $c = \infty$ are stable.

3. The effect of unequal diffusion coefficients on the wave speed at the Hopf bifurcation in the travelling wave equations

Eqs. (8) can be converted into a system of four first-order ordinary differential equations in the standard way, and linearising these equations about the steady state solutions of the reaction kinetics gives the characteristic equation

$$\begin{aligned} \text{Det}(J) &= \psi^4 + \psi^3 c_{\text{Hopf}}^2 \left(\frac{1}{\sqrt{\alpha}} + \sqrt{\alpha} \right) \\ &\quad + \psi^2 c_{\text{Hopf}}^2 \left(c_{\text{Hopf}}^2 + \sqrt{\alpha} f_U + \frac{g_V}{\sqrt{\alpha}} \right) \\ &\quad + \psi c_{\text{Hopf}}^4 (f_U + g_V) + c_{\text{Hopf}}^4 (f_U g_V - f_V g_U) \\ &= 0 \end{aligned} \quad (10)$$

where ψ is an eigenvalue of the stability matrix, the subscripts on f and g denote the partial derivatives with respect to U or V , evaluated at the steady state, and c_{Hopf} is the wave speed giving a Hopf bifurcation in (8). At c_{Hopf} , (10) will have a pair of pure imaginary roots, say $\psi = \pm i\zeta$, where ζ is the frequency of the corresponding (zero amplitude) travelling wave solution. Substituting these solutions into (10) and equating the real and imaginary parts gives

$$c_{\text{Hopf}} = \sqrt{\frac{-(g_V - \alpha f_U)^2 - f_V g_U (1 + \alpha)^2}{\sqrt{\alpha} (1 + \alpha) (f_U + g_V)}}. \quad (11)$$

This equation is not new, and was derived in a different way in Kopell and Howard's [9] original paper. Substituting the λ - ω kinetics (3) and (4), and the steady state $U = V = 0$, into (11) gives

$$c_{\text{Hopf}} = \sqrt{\frac{\omega_0^2 (\alpha + 1)^2 - (\alpha - 1)^2}{2\sqrt{\alpha} (\alpha + 1)}}, \quad (12)$$

which is plotted in Fig. 2(a) for different values of ω_0 . Straightforward analysis reveals that when $\omega_0 > 1$, $c_{\text{Hopf}} = +\infty$ at both $\alpha = 0$ and $\alpha = \infty$, and when $\omega_0 < 1$ c_{Hopf} is complex at both $\alpha = 0$ and $\alpha = \infty$. It is also straightforward to show that the curve described by Eq. (12) is symmetrical about $\alpha = 1$.

Substituting the predator-prey kinetics (9) and their steady state solutions into Eq. (11), with $\sigma = 0.15$ and $\mu = 0.05$,

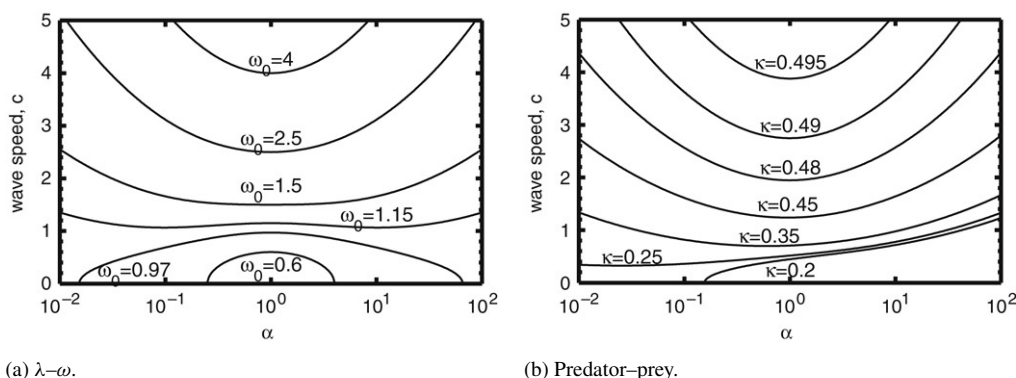


Fig. 2. The effect of varying α on the wave speed at the Hopf bifurcation, c_{Hopf} , for travelling wave equations (8) with reaction kinetics of λ - ω form (Eqs. (3) and (4)) (a) and with predator-prey reaction kinetics (Eqs. (9)) (b). (a) Different lines are realisations of Eq. (13) for different, labelled values of ω_0 , with $\omega_1 = 0.5$. (b) Different lines are realisations of Eq. (14) for different, labelled values of κ , with $\sigma = 0.15$ and $\mu = 0.05$.

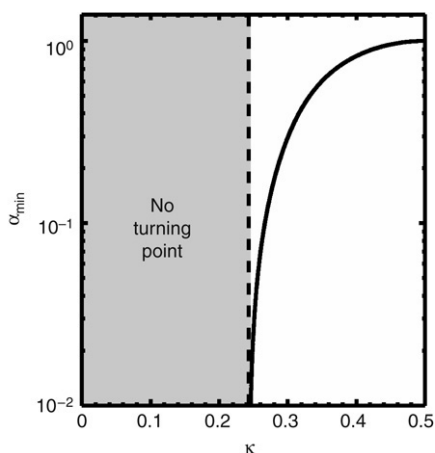


Fig. 3. The effect of varying κ on the value of α at the turning point of Eq. (13), α_{min} . Cycles occur in the region $0 < \kappa < 0.5$, but the turning point only occurs when $\kappa > \kappa_{\text{crit}} \approx 0.24$. The location of α_{min} provides a simple measure of the asymmetry in the effects of the two diffusion coefficients on the Hopf bifurcation wave speed c_{Hopf} .

gives

$$c_{\text{Hopf}} = \sqrt{\frac{3\alpha^2(\kappa - 2) + 6\alpha(\kappa - 2) + 14 - 77\kappa + 80\kappa^2}{60\sqrt{\alpha}(2\kappa - 1)(\alpha + 1)}}, \quad (13)$$

which is plotted in Fig. 2(b) for different values of κ . $c_{\text{Hopf}} = +\infty$ when $\alpha = \infty$ for all κ in the range $0 < \kappa < 0.5$. $c_{\text{Hopf}} = +\infty$ when $\alpha = 0$ for, and c_{Hopf} is complex when $\alpha = 0$ and $\kappa < \kappa_{\text{crit}}$. Differentiation of Eq. (13) with respect to α yields a cubic equation which indicates that when $\kappa > \kappa_{\text{crit}}$, Eq. (13) has one minimum, at α_{min} say. The deviation of α_{min} from 1 provides a simple measure of the asymmetry in the effects of the predator and prey diffusion coefficients on c_{Hopf} for different values of κ (Fig. 3). As $\kappa \rightarrow 0.5^-$ (Hopf bifurcation in the kinetics), the whole curve (13) becomes symmetrical about $\alpha = 1$. As κ is decreased below 0.5, α_{min} decreases, reflecting the greater asymmetry in (13) as the kinetics move further from Hopf bifurcation. Finally at $\kappa = \kappa_{\text{crit}}$, $\alpha_{\text{min}} = 0$; when $\kappa < \kappa_{\text{crit}}$ Eq. (13) has no turning points and c_{Hopf} doesn't exist for positive values of α sufficiently less than 1.

4. The effects of unequal diffusion coefficients on the wave family properties

4.1. Parameter ranges

For the λ - ω kinetics we fixed $\omega_1 = 0.5$ and picked three values for ω_0 ; a small ω_0 ($\omega_0 = 0.6$) where $\omega_0 < 1$, an intermediate ω_0 ($\omega_0 = 1.5$) where $\omega_0 > 1$, and a large ω_0 ($\omega_0 = 4$) which is also > 1 : recall that c_{Hopf} exists for all α if and only if $\omega_0 \geq 1$. In the normal form of an oscillatory system close to Hopf bifurcation, the parameter ω_0 is always large, being inversely proportional to the square of the limit cycle radius [14]; see Ref. [15] for the normal form derivation for Eqs. (9). However we chose to include our analysis of the other two cases, both for completeness and because they aid in the interpretation of the predator-prey cases.

For the predator-prey equations we considered four different values of the parameter κ . We chose $\kappa = 0.49$ and $\kappa = 0.4$ because they are reasonably close to the Hopf bifurcation of the kinetics (at $\kappa = 0.5$). When converted to normal form (see [15]), the corresponding λ - ω parameters are $\omega_1 \approx 0.86$ in both cases, with $\omega_0 \approx 47$ and $\omega_0 \approx 4.0$, respectively. The third case, $\kappa = 0.25$, was chosen because it is further from the Hopf bifurcation of the kinetics, but nevertheless c_{Hopf} exists for all values of α . The fourth case we studied was $\kappa = 0.2$, for which c_{Hopf} does not exist when $\alpha < 0.15$.

4.2. λ - ω kinetics

For both sets of kinetics, and for the chosen parameter sets, we confirmed the existence of a family of travelling waves for values of α between 0.01 and 100. These are plotted, in c - α and amplitude- α space in Figs. 4 and 5, with contour lines of fixed time period overlaid. These contours indicate that, in all cases, there is a sheet of periodic travelling wave solutions in c - α space, bounded above by $c = \infty$ (zero wave number), and bounded below by the Hopf bifurcation curve when this exists, or $c = 0$ when it doesn't.

For given parameters in the λ - ω kinetics, the effects of variation in α on the wave family properties is always symmetrical about $\alpha = 1$ (Fig. 4). The effects of varying

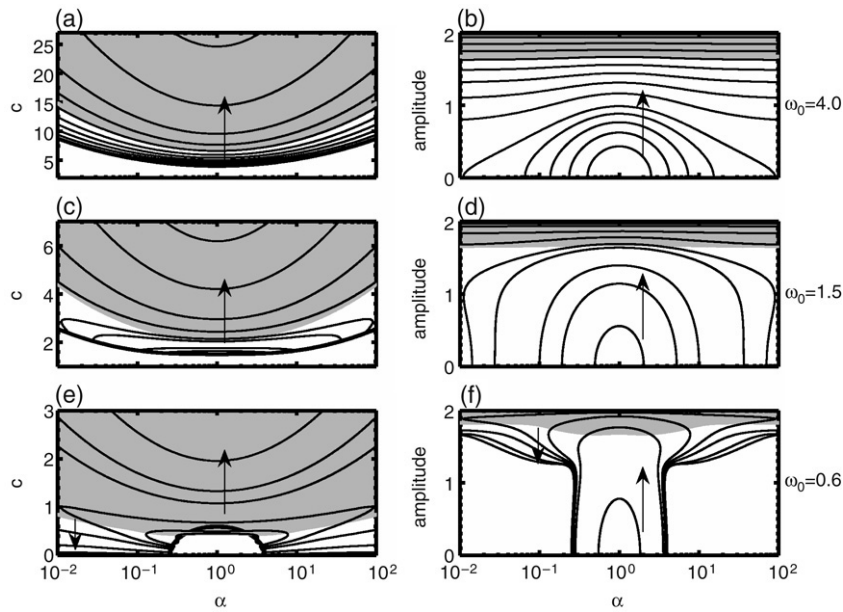


Fig. 4. The effect of varying α on the shape of the wave family and on wave stability when the kinetics of the travelling wave equations (8) are of λ - ω form (Eqs. (3) and (4)) and $\omega_1 = 0.5$. In (a) and (b) $\omega_0 = 4$, in (c) and (d) $\omega_0 = 1.5$, and in (e) and (f) $\omega_0 = 0.6$. Thick solid lines in (a), (c) and (e) are the locus of c_{Hopf} (Eq. (13)). Thin lines are contours of waves of specific periodicity. Arrows indicate the direction of contours of increasing periodicity. The region of stable waves is shaded in grey. The ranges of the time period contours are (a,b) 1.58–1.79, (c,d) 4.2–6.2 and (e,f) 11–62. In (a) and (c) some contours lie so close to the c_{Hopf} line as to be indistinguishable. Note the \log_{10} axis for α .

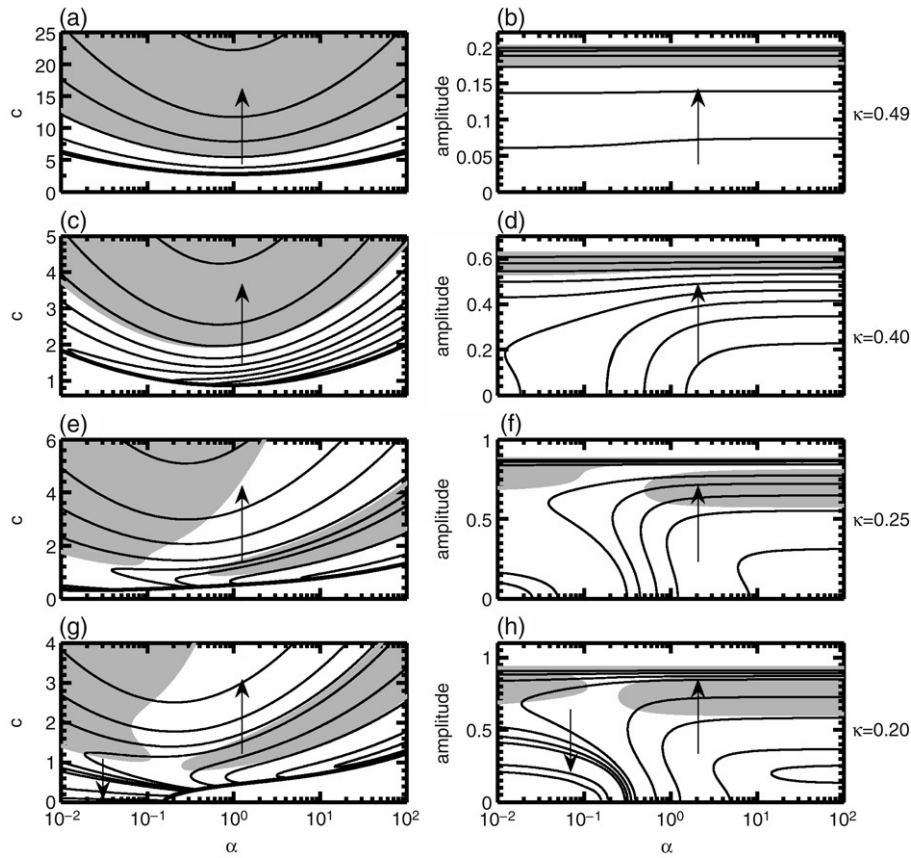


Fig. 5. The effect of varying α on the shape of the wave family and on wave stability when the kinetics of the travelling wave equations (8) are of the predator–prey form (Eqs. (9)). Parameter values are $\sigma = 0.15$, $\mu = 0.05$ and (a,b) $\kappa = 0.49$, (c,d) $\kappa = 0.40$, (e,f) $\kappa = 0.25$, and (g,h) $\kappa = 0.20$. Thick solid lines in (a), (c), (e) and (g) are the locus of c_{Hopf} (Eq. (14)). Thin lines are contours of waves of specific periodicity. The region of stable waves is shaded in grey. The ranges of the time period contours are (a,b) 39.6–40.3, (c,d) 38.5–47.5, (e,f) 39.0–140 and (g,h) 36.0–200. The arrows indicate the direction of contours of increasing periodicity. Note the \log_{10} axis for α .

α are relatively minor in the two cases in which $\omega_0 > 1$ (Fig. 4(a)–(d)). For all values of α , the minimum speed of the wave family is at c_{Hopf} , at which wave amplitude is zero. The branch of periodic solutions emerging from c_{Hopf} is always in the direction of increasing wave speed (and amplitude) in these cases. Time period also generally increases with wave speed and amplitude for a given α , with the exception of an initial decrease from the time period at c_{Hopf} when α is sufficiently smaller or larger than 1 (as is apparent in Fig. 4(c)). Stability analysis reveals a single critical value of speed and amplitude at which wave stability changes, for all values of α analysed, with low amplitude waves being unstable and high amplitude waves being stable. The shape of the stability boundary line has a similar shape to the nearby time period contours, implying that the time period at which stability changes has only a slight dependence on α . In summary, changing α has relatively little effect on the properties of the travelling wave family for these parameter values. The main effect of increasing (or decreasing) α away from $\alpha = 1$, in these scenarios, is to increase the speed, and decrease the amplitude, of waves of a given time period.

In the case in which $\omega_0 < 1$ (Fig. 4(e) and (f)) the effect of varying α on the shape of the wave family is similar to the two previous examples at the high wave speed end ($c > 1$, say). However, there are significant differences at slower wave speeds. In the region in which the c_{Hopf} line exists, wave speed initially decreases with increasing amplitude away from the Hopf bifurcation point, indicating a subcritical Hopf bifurcation. Increasing $|c - c_{\text{Hopf}}|$ is always associated with increasing time period in this region, causing certain wave speeds to be associated with two different time period values. The sheet of solutions in c – α space, in this scenario, therefore folds at a minimum wave speed (at $c < c_{\text{Hopf}}$) for some values of α . Where the c_{Hopf} line does not exist, the minimum wave speed is zero, which is associated with non-trivial stationary waves. As wave speed increases from zero, time period decreases from infinity, before reaching a minimum and then increasing again. In summary, varying α has a minor quantitative effect on the properties of the wave family at the high wave speed end in this scenario, and in a manner similar to the previous examples. At the low wave speed end of the wave family, increasing or decreasing α away from $\alpha = 1$ causes an increasingly large “tail” in the wave family in which wave speed and/or time period initially decrease before increasing with increasing distance from c_{Hopf} when this exists, and from $c = 0$ otherwise.

4.3. Predator–prey kinetics

For the predator prey kinetics, the effects of variation in α on the wave family properties are not generally symmetrical about $\alpha = 1$ (Fig. 5). The degree of asymmetry increases with decreasing κ . For our highest value of κ ($\kappa = 0.49$), in which the limit cycle of the kinetics is of low amplitude, the effects of variation in α is qualitatively very similar to the λ – ω scenarios when $\omega_0 > 1$ (Fig. 5(a) and (b) compared to Fig. 4(a)–(d)). When $\kappa = 0.4$ the asymmetry about $\alpha = 1$ is noticeable (Fig. 5(c) and (d)). Several lines of fixed time period

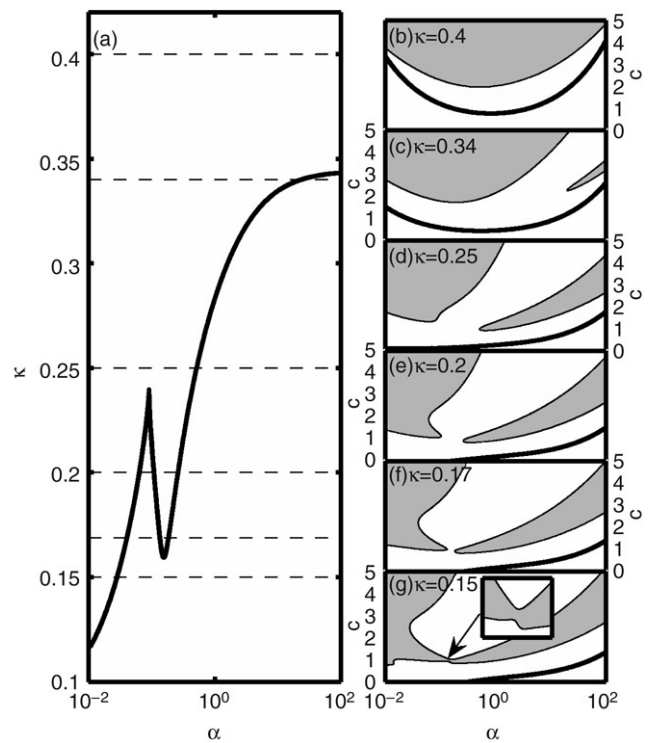


Fig. 6. (a) The α value associated with folds in the stability boundaries for varying κ when the kinetics of the travelling wave equations (8) are of the predator–prey form (Eqs. (9)) with $\sigma = 0.15$, $\mu = 0.05$. We have plotted α on the horizontal axis to aid interpretation and comparison with other figures. (b)–(g) show the stability boundaries for given values of κ , which are indicated by dashed lines in (a). The insert in (g) shows a close up of the region indicated by the arrow, to illustrate that there is a single region of wave stability.

only occur for sufficiently large α and the stability boundary is also asymmetrical about $\alpha = 1$. When $\kappa = 0.25$, the most obvious difference to the previous scenarios is that there are two separate regions of stability (Fig. 5(e) and (f)). The stability boundary in the previous scenarios has shifted to have a turning point at $\alpha \approx 0.025$ and there is now a second stability region. For c greater than about 1.5, the time period contours are similar to the previous scenarios, except that they have a minimum wave speed at α values of about 0.2. For c less than about 1.5, the time period contours fold at a certain wave speed which is greater than c_{Hopf} . The effects of α when $\kappa = 0.2$ are similar (Fig. 5(g) and (h)). The main difference from the $\kappa = 0.25$ case is that high wave period contours exist at low wave speeds when c_{Hopf} doesn't exist and, as for the λ – ω kinetics when $\omega_0 = 0.6$ (Fig. 4(e) and (f)), there is a non-zero minimum wave amplitude at $c = 0$ (Fig. 5(h)).

We investigated further the changes in the stability boundaries as κ varies by performing a continuation of the fold in the second region of wave stability (i.e. that with larger α values in Fig. 5(e)–(h)) (plotted in Fig. 6(a)). This fold corresponds to the smallest value of α in the second stability region. Fig. 6(b)–(g) show in more detail how the shapes and positions of the stability boundaries vary as κ is reduced from $\kappa = 0.4$. At $\kappa = 0.4$ there is only one region of stability. The second stability region appears from $\alpha = \infty$ and $c = \infty$ when $\kappa \approx 0.34$. As κ is reduced further, the region becomes larger,

while at $\kappa \approx 0.24$ two folds develop in the boundary of the first stability region. At $\kappa \approx 0.16$ the two stability boundaries meet, giving a single region of wave stability.

In summary, varying α can have relatively large effects on the properties of the wave families in the predator–prey scenarios. Most notably, varying α can dramatically alter the stability of waves of a given time period or wave speed. For example in the case where $\kappa = 0.2$, when $\alpha = 100$, stability is restricted to waves with either a speed that is small and within a narrow range of values, or a very fast speed; in contrast, when $\alpha = 0.01$, stable waves occur for all speeds above a minimum value. Furthermore, varying α can alter the range of wave properties that can be observed.

5. The effect of unequal diffusion coefficients on periodic travelling waves generated by Dirichlet boundary conditions

So far our analysis has concerned the effects of α on the shape of the one-parameter family of periodic travelling waves. In this, and the following, section we analyse how unequal diffusion coefficients affect the properties of the actual waves that arise in simulations of the reaction–diffusion equations (1). It is now well established that periodic travelling waves can arise naturally in reaction–diffusion systems in a variety of circumstances. Broadly these can be grouped into waves induced by (i) boundary conditions [16,17]; (ii) “invasion”, whereby an unstable steady state ahead of an invasion front changes to periodic travelling waves behind the invasion front [18–25]; and (iii) heterogeneities in the environment [26–28]. In this section we focus on (i), and study (ii) in the next section.

We performed simulations of Eqs. (1), for two of the cases studied in the previous section, on a one dimensional domain with $u = v = 0$ at one boundary and $\partial u/\partial x = \partial v/\partial x = 0$ at the other. All simulations started with random initial values for u and v . The zero Dirichlet condition forces the system away from spatially uniform oscillations and in all cases the long-term solution consisted of a periodic travelling wave over at least part of the domain, with thin transition layers near the boundaries. Fig. 1(c) and (d) are two example realisations of these simulations. We calculated numerically the speed, space and time periods, and amplitude of the wave (since these are commonly measured in ecological studies), and our results are shown in Fig. 7. To aid interpretation of these results we display them in combination with curves that define the range of possible values for the wave family properties. These lines were determined using the same techniques described in the previous section except that to calculate the spatial wavelength contours we substituted the alternative travelling wave coordinate $\hat{z} = x - ct$ into Eqs. (1) and used AUTO to analyse the resultant travelling wave equations.

The mechanism via which a Dirichlet boundary condition selects a particular member of the periodic travelling wave family has been studied in detail in previous papers [15–17], and we will not attempt to refine or extend these studies here. Rather, our objective is to use our results on the

properties of the wave family to give a clearer interpretation of the observed behaviour, in particular the occurrence of spatiotemporal irregularities.

5.1. λ – ω kinetics

The effects of α on the overall range of possible wave properties predicted by Eqs. (8) with the λ – ω kinetics Eqs. (3) and (4) is, as suggested in the previous section, relatively minor and symmetrical about $\alpha = 1$ (Fig. 7 (a,c,e,g)). For all values of α there is a band of unstable solutions close to the Hopf bifurcation and a single boundary at which stability changes. Our numerical simulations predict stable travelling waves for all values of α in this scenario. In all cases, the time periods and amplitudes of the travelling waves are close to those of the limit cycle of the kinetics (Fig. 7(a,c,e,g)). The effects of varying α on the properties of the waves selected by these boundary conditions are similar to the effects of α on the shapes of various wave family properties. In particular, the minimum of all wave properties shown in Fig. 7 (a,c,e,g) occurs at $\alpha = 1$ and the effects of changing α is symmetrical about this point.

5.2. Predator–prey kinetics

The effects of α on the overall range of possible wave properties predicted by Eqs. (8) with the predator–prey kinetics Eqs. (9) are asymmetrical about $\alpha = 1$ in this scenario (Fig. 7(b, d, f, h)). In the region where c_{Hopf} doesn't exist, we found that the wavelength and amplitude approach non-zero minimum values as $c \rightarrow 0$. In Fig. 5(g) the largest time period that we plotted had a period of 200 and wave speed of about 0.1; wave amplitude varies smoothly with α along the contour. However, along contours of higher fixed time period, with wave speeds less than about 0.01, there are ‘tongues’ in the plots of amplitude and wavelength against α (not visible in the wavelength plot at the scale shown). In Fig. 7(f,h) we plot lines corresponding to the smallest value of c we used ($c = 6.5 \times 10^{-6}$). Further analysis reveals that these lines lie within a region of stationary patterned solutions. We omit more details of this region here for brevity but have included further information and analysis in the Appendix.

In this scenario there are two stability regions (Fig. 7(b, d, f, h)). The properties of the travelling waves picked out by the zero Dirichlet boundary conditions in our partial differential equation simulations lie close to these stability boundaries. In fact, in some cases, the selected travelling waves lie on the unstable side of the stability boundary. Our numerical simulations showed that, in all of these cases, the travelling waves that formed behind the Dirichlet boundary conditions eventually developed into irregular spatiotemporal behaviour (such as in Fig. 1(d), for example). Varying α also has a significant effect on the measured properties of waves arising in these scenarios, with a minimum generally occurring close to $\alpha = 1$. Varying α can therefore have significant effects on the properties of the waves selected by these boundary conditions.

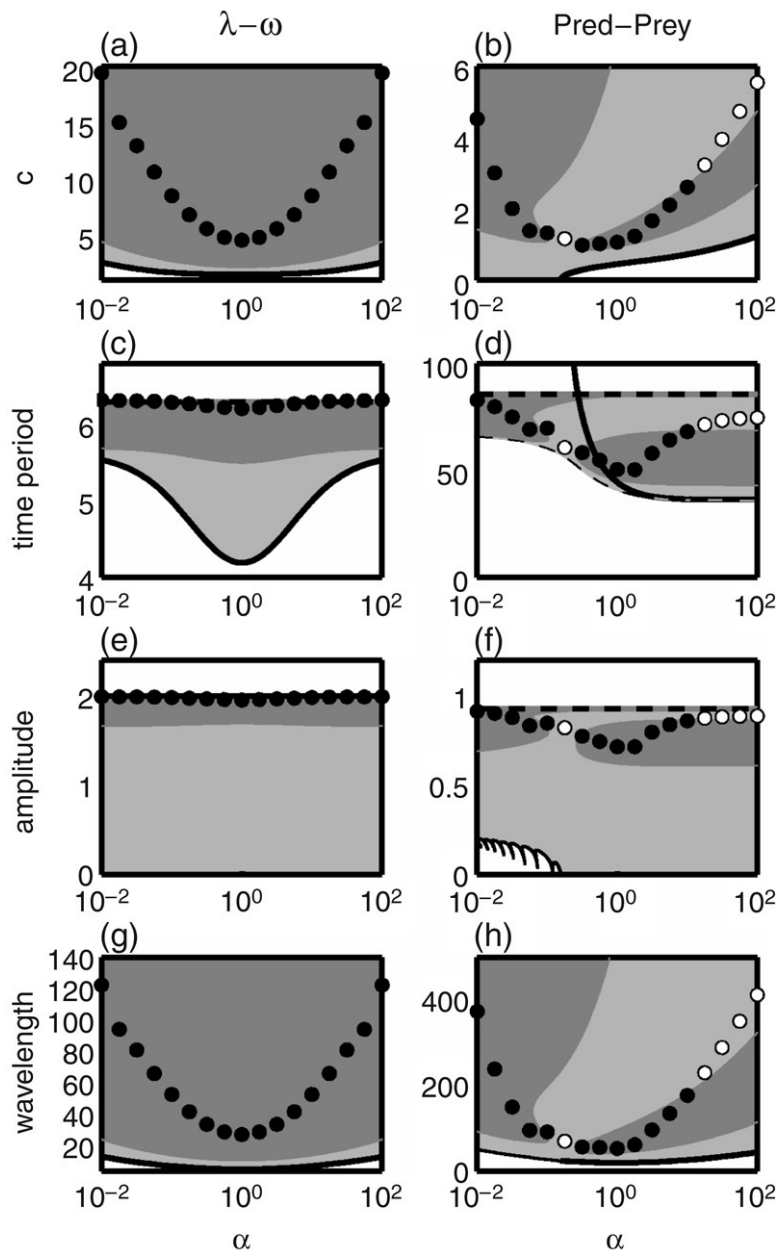


Fig. 7. The effect of α on the maximum and minimum values of the wave properties in the travelling wave family (solutions of Eqs. (8)), and on the wave properties picked out by zero Dirichlet boundary conditions in simulations of Eqs. (1), for different reaction kinetics. Column headings correspond to $\lambda-\omega$ kinetics (Eqs. (3) and (4) with $\omega_1 = 0.5$ and $\omega_0 = 1.5$), and to predator–prey kinetics (Eqs. (9) with $\sigma = 0.15$, $\mu = 0.05$ and $\kappa = 0.2$). Light shaded areas denote the region of unstable travelling waves and dark shaded areas denote the region of stable travelling waves; in unshaded areas there are no travelling waves. Lines correspond to the positions of the Hopf bifurcation of the wave family (thick solid), a fold in the wave family (thin dashed), the value corresponding to the limit cycle of the kinetic equations (thick dashed) or the value at the locus of waves of specific periodicity (thin solid line—see text for explanation). Circles correspond to the values predicted by simulations of Eqs. (1), solved numerically as detailed in Section 5. Filled circles denote waves that showed no evidence of instability. Open circles denote waves that existed transiently before developing into irregular spatiotemporal behaviour. Spatiotemporal dynamics for two scenarios with predator–prey kinetics, when $\alpha = 1$ and $\alpha = 100$, are shown in Fig. 1(c) and (d), respectively. Values reported for apparently unstable periodic travelling waves were measured from the region of waves that form directly behind the Dirichlet boundary, as is visible in Fig. 1(d). Note the \log_{10} axis for α .

6. The effect of unequal diffusion coefficients on periodic travelling waves generated by predators invading a prey population

For our second case study we analyse the effects of changing the diffusion coefficients on the waves generated by a predators invading a prey population. This situation, which has no analogue for the $\lambda-\omega$ kinetics, has been studied in detail in the

case of equal predator and prey diffusion coefficients [21,29, 35]. However, changing the ratio of the diffusion coefficients enables a more comprehensive comparison of the invasion speed, and the speed of periodic waves behind the invasion. Again, our focus is on the use of our wave family study to interpret the results of partial differential equation simulations, rather than on the underlying wave selection mechanism,

which is discussed in detail elsewhere [35]. We conducted a limited study of such invasions by simulating Eqs. (1) with predator–prey kinetic Eqs. (9). Our boundary conditions were $\partial u/\partial x = \partial v/\partial x = 0$ at both ends of a large domain and we used initial conditions of $u = 1, v = 0$ across the whole domain except at the left boundary where $u = 1$ and $v = 1$. We chose two parameter sets, one in which the limit cycle of the kinetics is close to Hopf bifurcation ($\kappa = 0.49$) and one in which it is far from Hopf bifurcation ($\kappa = 0.2$). Rather than fixing $\beta = \sqrt{D_u D_v}$ and varying $\alpha = \sqrt{D_u/D_v}$ in Eqs. (1), as in the rest of the paper, it is more convenient to do numerical simulations with a fixed value of D_v . This fixes the invasion speed, and thus allows us to fix an appropriate domain size. We then varied $\alpha = D_u$. Effectively, this is a rescaling of the wave speed. However, for consistency with the rest of the paper, we undo this rescaling before plotting wave speeds calculated from our simulations.

In Fig. 8 we give examples of the emergent spatiotemporal dynamics and in Fig. 9 we plot the measured speeds of periodic waves behind the invasion front for differing values of α . As discussed above, we have reversed our rescaling of wave speed in Fig. 9 to maintain consistency with the previous sections. In the case where the kinetics are near Hopf bifurcation, we found that α values greater than about 0.1 generated periodic waves travelling in the opposite direction to the invasion front, sometimes with a region of spatiotemporal irregularities behind the front (Figs. 8(b), 9(a)). For these values of α , the selected waves lie close to the stability boundary, but within the stable region. For α less than about 0.1 we found no stable periodic travelling waves, and instead apparently irregular spatiotemporal behaviour develops immediately behind the invasion front (Figs. 8(c), 9(a)). It was therefore not possible to estimate the speed of selected periodic solutions in these scenarios. Similar dynamics were also predicted for a narrow region of α values close to 1.6. Presumably in these cases the selected wave lies in the unstable region.

When the kinetics are far from Hopf bifurcation, we found that sufficiently high values of α also selected stable waves travelling away from the invasion front (Figs. 8(a), 9(b)). Simulations in which α lies between about 0.1 and 1 gave travelling waves that eventually decayed to irregular spatiotemporal behaviour. This is consistent with our stability calculations, since the measured wave speeds fall within a region of the graph corresponding to unstable waves (Fig. 9(b)). These values of α are also associated with the appearance of a region of small amplitude and short wavelength waves moving in the direction of the invasion front and at the same speed (shown in the insert in Fig. 8(d)). Where $\alpha \leq 0.1$, two regions of stable travelling waves develop behind the invasion front (Figs. 8(d), 9(b)). A region of low amplitude stable waves, with a low wave speed, develops immediately behind the invasion front and a region of higher amplitude, faster waves develops from the left boundary. As time progresses the high amplitude fast waves invade the region of low amplitude slow waves but at a rate that is slower than the invasion, so that the regions occupied by the two periodic waves both grow in extent.

One by-product of our stability calculations is that we also obtain the group velocity (the speed with which a perturbation to the wave travels [33,44]) on the stability boundary. It is straightforward to use this as a starting point for numerical continuation of group velocity. This shows that throughout parameter space in Fig. 9(b) the group velocity is negative.

The results in the previous sections allow us explain these results to some extent. We know that the minimum possible travelling wave speed is c_{Hopf} when it exists and zero when it doesn't (Fig. 2(b)). Moreover, simple linearization ahead of the invasion suggests that the speed of the invasion front, c_{Inv} , may be given by

$$c_{\text{Inv}} = 2 \left[D_v \left. \frac{\partial g}{\partial v} \right|_{u=1, v=0} \right]^{\frac{1}{2}} = 2 \left[D_v \left(\frac{\sigma}{1 + \kappa} - \mu \right) \right]^{\frac{1}{2}}. \quad (14)$$

Although front propagation speeds depend on nonlinearities in some reaction–diffusion systems (see for example [40]) extensive numerical simulations confirm Eq. (14) as the invasion speed for our system. These two wave speeds are superimposed on our simulation results in Fig. 9. For the parameter values used in Fig. 9(a), $c_{\text{Hopf}} > c_{\text{Inv}}$ for all values of α , and when periodic waves develop, they always move at a faster speed than the invasion. When α is less than about 0.1 our numerical simulations predict highly irregular spatiotemporal oscillations such as those shown in Fig. 8(c). In previous papers [37], the selection of unstable waves by invasion has been postulated as a mechanism for generating spatiotemporal chaos but discussions have been very speculative due to an absence of precise information on wave stability.

In Fig. 9(b), $c_{\text{Hopf}} < c_{\text{Inv}}$ for smaller α , and correspondingly two new phenomena occur. Firstly, as α decreases below about 1, a band of periodic waves develops immediately behind the invasion front, moving at the same speed. For large α , the initial invasion has the form of a transition wave connecting $u = 1, v = 0$ and $u = u_s, v = v_s$ (shown most clearly in Fig. 8(b,c), which are for larger κ). This transition wave is effectively a heteroclinic connection in the travelling wave equations (8) with $c = c_{\text{Inv}}$. As α decreases through about 1.5, c_{Hopf} decreases below c_{Inv} , and the eigenvalues of (8, $c = c_{\text{Inv}}$) change to all having negative real parts. No heteroclinic connection is therefore possible, and our simulations suggest that instead, the initial invasion occurs via a point-to-periodic orbit connection. For α just below 1.5, the periodic waves moving with invasion speed are unstable and are seen only transiently, with the long-term behaviour being spatiotemporal irregularity. However for α less than about 0.1, the waves are stable and persist. In addition, for α less than about 0.1, a second band of periodic waves develops from the $x = 0$ boundary, of higher amplitude and faster speed than those moving with the invasion. This second band of waves is a new phenomenon, not reported in previous work on invasion in oscillatory predator–prey systems (which is for $\alpha = 1$). We speculate that the interaction of the low amplitude waves and the Neumann boundary conditions at $x = 0$ selects for stable wave trains which propagate in the direction of the invasion, but beyond this we have no clear explanation.

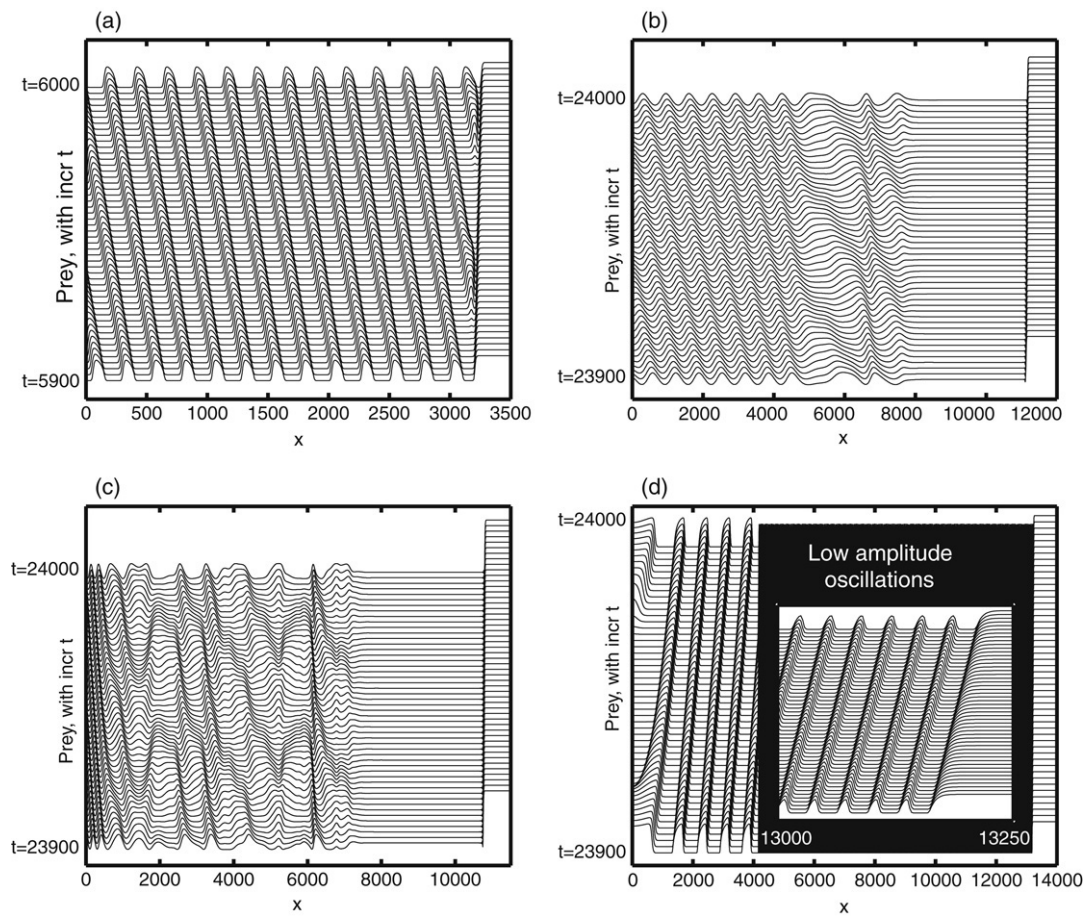


Fig. 8. Simulation of the invasion of a prey population by predators using Eqs. (1) with predator–prey reaction kinetics (9), and with $\sigma = 0.15$, $\mu = 0.05$ and $D_v = 1$. In (a) and (d) the limit cycle of the kinetics is far from the Hopf bifurcation ($\kappa = 0.2$), and in (b) and (c) it is close to the Hopf bifurcation ($\kappa = 0.49$). Prey diffusion coefficients are (a) $D_u = 1$, (b) $D_u = 2.5$, (c) $D_u = 0.004$, and (d) $D_u = 0.1$. The region of low amplitude oscillations behind, and moving with, the invasion front in (d) are indistinguishable at the scale shown due to their short wavelength (appearing as a black block). The insert in (d), laid on top of this region, shows a close up of the region just behind the invasion front, plotted over the same time interval as the main figure. The equations were solved numerically as detailed in Section 6. We assume zero Neumann boundary conditions at both boundaries.

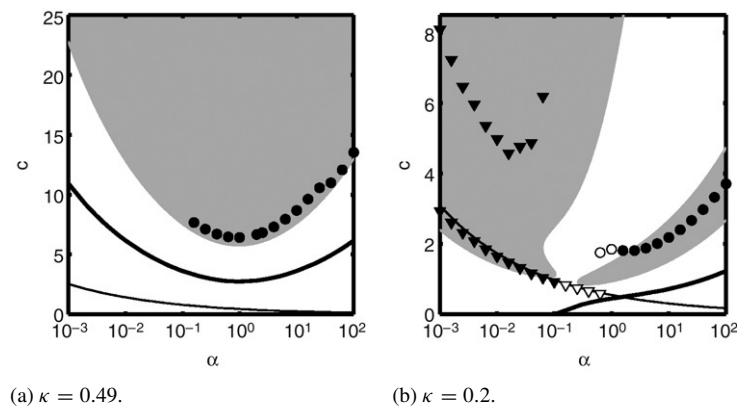


Fig. 9. The effects of varying $\alpha = D_u$ on the speed of the travelling waves emerging behind the invasion front (dots and triangles) in numerical simulations of Eqs. (1) with reaction kinetics (9), and with $\sigma = 0.15$, $\mu = 0.05$ and $D_v = 1$. In (a) the limit cycle of the kinetics is close to the Hopf bifurcation ($\kappa = 0.49$), and in (b) it is far from the Hopf bifurcation ($\kappa = 0.2$). Dots represent negative wave speeds (travelling in the opposite direction to the invasion front) and triangles represent positive wave speeds (travelling in the direction of the invasion front). Filled symbols denote waves that showed no evidence of instability. Open symbols denote waves that developed into irregular spatiotemporal behaviour. The equations were solved numerically as detailed in Section 6. In addition we have plotted c_{Hopf} (thick line) and the invasion wave speed c_{inv} (thin line), calculated using Eqs. (13) and (14), respectively. For consistency with the rest of the paper, the wave speeds calculated from our simulations have been rescaled (see text). Note that in (a) it was not possible to estimate the speed of selected periodic solutions when $\alpha \leq 0.1$: these simulations predicted highly irregular spatiotemporal dynamics behind the invasion front.

7. Discussion

In 1973, Kopell and Howard [9] published their landmark paper on periodic travelling wave solutions of oscillatory reaction–diffusion equations. They proved that for any set of parameters for which the travelling wave ordinary differential equations have a Hopf bifurcation, there is a one-parameter family of such wave solutions. They also proved that low amplitude waves are unstable provided that the diffusion coefficients are sufficiently close. Further they introduced and analysed in detail the λ – ω class of reaction–diffusion equations, which have become important prototype equations for the study of periodic travelling waves and other spatiotemporal phenomena. Our philosophy in this paper has been to investigate numerically a variety of extensions to Kopell and Howard’s work using numerical continuation methods. This has given a comprehensive picture of the way in which wavelength, amplitude, speed, time period and stability vary along the wave family, for a number of sets of kinetic terms. Crucially, our results include variations in the ratio of diffusion coefficients; this is an important extension, since many results of Kopell and Howard and subsequent authors apply only to the case of equal diffusion coefficients. In particular our results lead us to hypothesise that a one-parameter family of travelling waves exists for all combinations of diffusion coefficients (except the trivial case where both are equal to zero), even though the Hopf bifurcation from which the wave family emerges may not exist for all ratios of diffusion coefficients.

Kopell and Howard’s results on wave stability, and those of subsequent authors, are restricted to waves of sufficiently high or low amplitude, except for the exact criterion for wave stability (6) in the λ – ω case. In that case, there are critical values of wave amplitude, speed and wavelength, below which waves are unstable and above which they are stable. Our results suggest that this simple division into stable and unstable waves applies generally for the λ – ω kinetics, for a wide range of ratios of the diffusion coefficients. However our results show that for other sets of kinetic terms this simple division may not apply, even with equal diffusion coefficients. Rather, there can in general be isolated bands of stable speed/amplitude.

From the viewpoint of applications to ecological systems our results have several important implications. The first is that the ratio of the diffusion coefficients could have important effects on the wave family properties, and on the properties of waves picked out by given initial and boundary conditions. For example, in the predator prey scenario, the range of wavelengths picked out by Dirichlet boundary conditions, as a function of α , varies over 8-fold (Fig. 7(h)). This could determine whether or not waves can be detected in a domain (habitat) of limited size, or with limited resources available for spatiotemporal data gathering. If the observed spatiotemporal oscillations are of low amplitude (relative to their mean), then we predict that the effects of changing the diffusion coefficients should be similar to our findings for the λ – ω kinetics above, and should be independent of the actual underlying kinetics. However, the presence of fluctuations induced by environmental factors and measurement error may

make it impossible to detect periodic travelling waves of such low amplitude. For higher amplitude oscillations, predictions on the effects of changing the diffusion coefficients are not possible without some knowledge of the kinetic equations.

Thus far, we have not analysed the wave family properties as $\alpha \rightarrow \infty$ or as $\alpha \rightarrow 0$. The latter limit is of direct ecological relevance, giving a model for plant–herbivore interaction. In a number of other reaction–diffusion systems [38,42,43], periodic travelling waves approach a repeating series of increasingly localised spikes as the ratio of the diffusion coefficients tends to zero or infinity. The $\alpha \rightarrow \infty$ and $\alpha \rightarrow 0$ limits are of course singular for the travelling wave Eqs. (8). However, it is straightforward to construct travelling wave equations for the limiting cases $D_u = 0$ ($\alpha = 0$) and $D_v = 0$ ($\alpha = \infty$), and wave families can be found by numerical continuation of these third-order systems. A relatively limited study for the predator–prey kinetics, using this approach, suggests that the periodic travelling waves are not localised in these limiting cases, and that the $\alpha \rightarrow \infty$ and $\alpha \rightarrow 0$ limits are regular for the periodic travelling wave solutions.

A surprising finding in our investigation of wave stability is that, in all cases we studied, wave stability only changes through an Eckhaus (‘sideband’) instability, and not through a Hopf bifurcation, in contrast to [38]. Exploring the scenarios under which these two different types of instability occur is a natural direction for future study.

The results presented here are one step towards understanding, and possibly predicting, the properties of the spatiotemporal dynamics that emerge from particular initial or boundary conditions in oscillatory ecological systems. Our analysis of the waves selected by zero Dirichlet boundary conditions has shown that changing the diffusion rates can influence the properties of the resulting periodic travelling waves, including their stability. Previous studies of such wave selection have been restricted to equal diffusion coefficients [15–17]. Here, we extend this work, demonstrating that the diffusion coefficients play a key role in wave selection, including the stability of the selected wave and consequently whether the long-term spatiotemporal dynamics are ordered or disordered. Our stability analysis is based on the essential spectrum, and this applies on unbounded domains. As shown in Fig. 1(d), however, waves that are essentially unstable may nevertheless be stable on sufficiently small bounded domains. The results shown in Fig. 1(d) suggest that the periodic travelling waves selected in this case are convectively unstable [36], with the perturbation generated by the zero Dirichlet boundary conditions being convected to the right whilst growing. As a result, the waves only visibly “break up” at sufficient distance from the boundary. A natural extension of our work would be a comprehensive study of when the essentially unstable waves are also absolutely unstable (implying instability on all sufficiently large domains) [36]. Such a study would clarify, for example, why there are values of α in Fig. 9(a) that predict highly irregular spatiotemporal dynamics without any evidence of periodic travelling waves, whereas in Fig. 9(b), irregularities occur behind bands of essentially unstable waves.

Acknowledgements

M.J.S. was supported by a Natural Environment Research Council (NERC) Environmental Mathematics and Statistics studentship. J.A.S. was supported in part by an Engineering and Physical Sciences Research Council (EPSRC) Advanced Research Fellowship. We thank Xavier Lambin (Aberdeen), Gabriel Lord (Heriot-Watt), Simon Malham (Heriot-Watt), Jens Rademacher (CWI, Amsterdam), Bjorn Sandstede (Surrey), two anonymous reviewers and the participants and organisers of the "Travelling Waves: Theory and Applications" workshop (26–30 March 2007, Surrey University) for helpful advice and discussions. We also thank the authors of the AUTO package [11–13], without which this study would not have been done.

Appendix

In this appendix we provide further details on the stationary patterned solutions that are approached in the predator–prey reaction diffusion equations (Eqs. (1) with kinetics (9), and $\sigma = 0.15$, $\mu = 0.05$ and $\kappa = 0.2$), when $\alpha < \alpha_{\text{crit}} \cong 0.15$, as $c \rightarrow 0$ (Fig. 7(f,h)).

We substituted the alternative travelling wave coordinate $\hat{z} = x - ct$ into Eqs. (1) to allow us to investigate the travelling wave contours when c is close to zero. We found that for any given value of $\alpha < \alpha_{\text{crit}}$ with other parameters as above, wavelength and amplitude approach non-zero limiting values as $c \rightarrow 0$ (Fig. A.1). This implies that there are limiting curves of minimum wavelength and amplitude for $\alpha < \alpha_{\text{crit}}$ and these curves were estimated using AUTO by fixing c at a very small, non-zero value and continuing in α (Fig. A.2).

Fig. A.2 illustrates that this limiting curve (also illustrated in Fig. 6) is non-monotonic, exhibiting 'tongues'. That is, regions in which there are a series of sharp amplitude decreases and increases for small changes in α .

Stationary patterns satisfy the equations

$$0 = \sqrt{\alpha} \frac{\partial^2 u}{\partial x^2} + f(u, v) \tag{A.1a}$$

$$0 = \frac{1}{\sqrt{\alpha}} \frac{\partial^2 v}{\partial x^2} + g(u, v). \tag{A.1b}$$

Equations of this form are well studied in the case of Turing patterns (e.g. [1]) and although our system is not a Turing system the analysis of it is very similar. We first linearise the equations about their steady states with $\tilde{u} = u - u_s$ and $\tilde{v} = v - v_s$ and then separate the solutions into Fourier modes: $\tilde{u} = u_0 e^{ikx}$ and $\tilde{v} = v_0 e^{ikx}$. Substituting these into the linearised equations gives

$$0 = u_0 (f_u - K\sqrt{\alpha}) + v_0 f_v \tag{A.2a}$$

$$0 = v_0 (g_v - K(1/\sqrt{\alpha})) + u_0 g_u \tag{A.2b}$$

where $K = k^2$, and hence,

$$K^2 - K(\sqrt{\alpha} + 1/\sqrt{\alpha}) + f_u g_v - f_v g_u = 0. \tag{A.3}$$

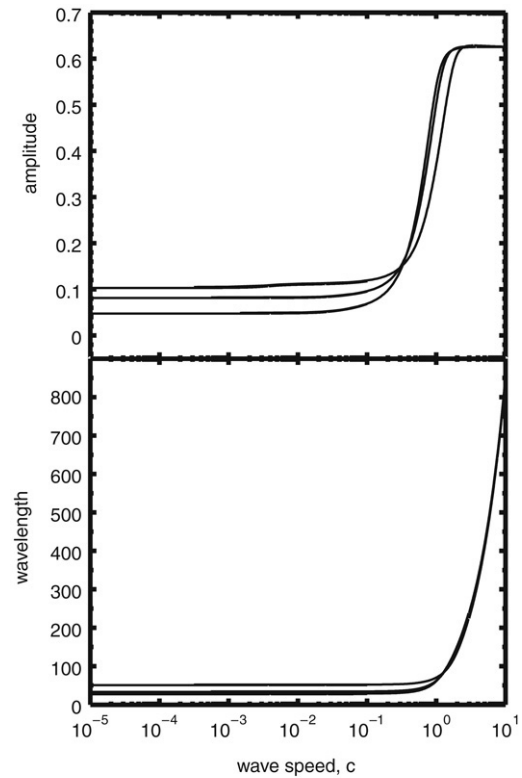


Fig. A.1. The effect of reducing wave speed towards zero on wave amplitude and wavelength for three different values of $\alpha < \alpha_{\text{crit}}$ (see text for equations and parameters). These results demonstrate that amplitude and wavelength approach limiting values as $c \rightarrow 0$. The different lines correspond to $\alpha = 0.1$, $\alpha = 0.05$ and $\alpha = 0.01$, in order of decreasing asymptotic values of amplitude and wavelength as $c \rightarrow 0$. Note the \log_{10} axis for wave speed.

For stationary patterns to exist, this quadratic equation in K must have real roots, which requires that

$$(\sqrt{\alpha} + 1/\sqrt{\alpha})^2 - 4(f_u g_v - f_v g_u) > 0. \tag{A.4}$$

Since $f_u g_v - f_v g_u > 0$ for the parameter values we are using, there are two positive real roots for K whenever (A.4) is satisfied. Substituting the predator–prey reaction kinetics and parameter values into (A.4) gives the condition for stationary patterned solutions to exist as $\alpha < 1/3$.

To explore this patterned region we converted Eqs. (A.1) into four ordinary differential equations and studied this system of equations as a boundary value problem with $u(0) = u(L)$, $v(0) = v(L)$, $du/dx(0) = du/dx(L)$ and $dv/dx(0) = dv/dx(L)$ where L is the size of the domain.

We started with low amplitude sinusoidal stationary patterns as initial conditions. These were calculated by solving (A.3) for K , with all the other parameters specified, giving two values of K , K_1 and K_2 . The initial, low amplitude solutions at the specified value of α were then calculated using $u = u_s + u_0 \cos(\sqrt{K}x)$ and $v = v_s + v_0 \cos(\sqrt{K}x)$, where $u_0/v_0 = -f_v/(f_u - K\sqrt{\alpha})$. Strictly, these are only solutions in the limit as $u_0, v_0 \rightarrow 0$, but with small non-zero values of u_0 and v_0 , they are sufficiently accurate to provide a starting point for numerical continuation. We used AUTO to perform continuations of these solutions in α for different fixed

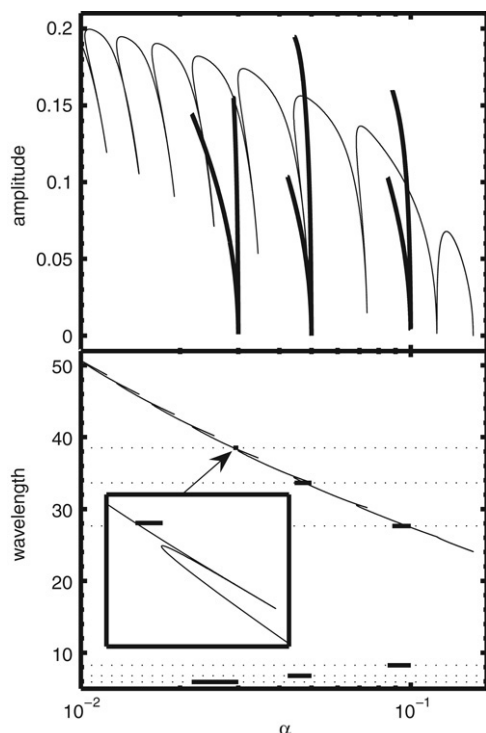


Fig. A.2. The limiting contour lines (thin) of amplitude and wavelength when $\alpha < \alpha_{\text{crit}}$ for the particular predator–prey scenario detailed in the text. The thick lines denote stationary patterned solutions of fixed wavelength predicted by Eqs. (A.1) and the dotted lines in the bottom panel are to highlight these wavelengths. The insert is a close up of the area indicated by the arrow, highlighting one of the “tongues” in the wavelength curve and one line of patterned solutions of fixed wavelength. Note the \log_{10} axis for α .

wavelengths (Fig. A.2). For each starting value of $\alpha (< \alpha_{\text{crit}})$, this continuation generates a curve of stationary patterns for both of the two fixed wavelengths. Moreover, both of these curves cross the limiting contours of periodic travelling wave amplitude as $c \rightarrow \infty$; one of these crossings corresponds to the limiting wavelength of the periodic travelling waves as $c \rightarrow 0$ (Fig. A.2, bottom panel).

These results show that there is a region of the amplitude– α plane in which there are stationary patterns; moreover there are exactly two stationary patterns, with different wavelengths, at each point in the region. The limiting forms of the periodic travelling waves as $c \rightarrow 0$ traces out a curve lying within this region.

References

- [1] J.D. Murray, *Mathematical Biology I: An Introduction*, third ed., Springer, Berlin, 2002.
- [2] J. Sneyd, J. Keitzer, M.J. Sanderson, *FASEB J.* 9 (1995) 1463.
- [3] T. Hofer, *Biophys. J.* 77 (1999) 1244.
- [4] Y. Timofeeva, S. Coombes, *J. Math. Biol.* 47 (2003) 249.
- [5] X. Lambin, D.A. Elston, S.J. Petty, J.L. MacKinnon, *Proc. R. Soc. Lond. B* 265 (1998) 1491.
- [6] J.L. MacKinnon, X. Lambin, D.A. Elston, C.J. Thomas, T.N. Sherratt, S.J. Petty, *J. Anim. Ecol.* 69 (2001) 106.
- [7] P. Giraudoux, P. Delattre, M. Habert, J.P. Quere, S. Deblay, R. Defaut, R. Duhamel, M.F. Moissenet, D. Salvi, D. Truchetet, *Agr. Ecosyst. Environ.* 66 (1997) 47.
- [8] O.N. Bjørnstad, M. Peltonen, A.M. Liebhold, W. Baltensweiler, *Science* 298 (2002) 1020.
- [9] N. Kopell, L.N. Howard, *Stud. Appl. Math.* 52 (1973) 291.
- [10] D. Cope, *SIAM J. Appl. Math.* 38 (1980) 457.
- [11] E.J. Doedel, *Cong. Numer.* 30 (1981) 265.
- [12] E.J. Doedel, H.B. Keller, J.P. Kernévez, *Internat. J. Bifur. Chaos* 1 (1991) 493.
- [13] E.J. Doedel, H.B. Keller, J.P. Kernévez, *Internat. J. Bifur. Chaos* 1 (1991) 745.
- [14] J. Guckenheimer, P. Holmes, *Nonlinear Oscillations, Dynamical Systems, and Bifurcations of Vector Fields*, Springer, New York, 1983.
- [15] J.A. Sherratt, X. Lambin, T.N. Sherratt, *Am. Nat.* 162 (2003) 503.
- [16] J.F.G. Auchmuly, G. Nicolis, *Bull. Math. Biol.* 38 (1976) 325.
- [17] J.A. Sherratt, *SIAM J. Appl. Math.* 63 (2003) 1520.
- [18] J.A. Sherratt, *SIAM J. Appl. Math.* 54 (1994) 1374.
- [19] J.A. Sherratt, *Physica D* 70 (1994) 370.
- [20] G.B. Ermentrout, X. Chen, Z. Chen, *Physica D* 108 (1997) 147.
- [21] J.A. Sherratt, M.A. Lewis, A.C. Fowler, *PNAS* 92 (1995) 2524.
- [22] S.V. Petrovskii, H. Malchow, *Math. Comput. Modelling* 29 (1999) 49.
- [23] S.V. Petrovskii, H. Malchow, *Nonlinear Anal. RWA* 1 (1999) 37.
- [24] P. Ashwin, M.V. Bartuccelli, T.J. Bridges, S.A. Gourley, *Z. Angew. Math. Phys.* 53 (2002) 103.
- [25] M.R. Garvie, *Bull. Math. Biol.* 69 (2007) 931.
- [26] P.S. Hagan, *Adv. Appl. Math.* 2 (1981) 400.
- [27] N. Kopell, *Adv. Appl. Math.* 2 (1981) 389.
- [28] A.L. Kay, J.A. Sherratt, *SIAM J. Appl. Math.* 61 (2000) 1013.
- [29] J.A. Sherratt, *Ecol. Lett.* 4 (2001) 30.
- [30] J.A. Sherratt, *Forma* 11 (1996) 61.
- [31] P. Turchin, *Complex population dynamics: A theoretical/empirical synthesis*, in: *Monographs in Population Biology*, vol. 35, Princeton University Press, Princeton, 2003.
- [32] N.F. Britton, *Reaction–Diffusion Equations and their Applications to Biology*, Academic, New York, 1986.
- [33] J.D.M. Rademacher, B. Sandstede, A. Scheel, *Physica D* 229 (2007) 166.
- [34] L.S. Tuckerman, D. Barkley, *Physica D* 46 (1990) 57.
- [35] J.A. Sherratt, *Physica D* 117 (1998) 145.
- [36] B. Sandstede, A. Scheel, *Physica D* 145 (2000) 233.
- [37] J.A. Sherratt, M.A. Lewis, A.C. Fowler, *PNAS* 92 (1995) 2524.
- [38] G. Bardiougov, H. Engel, *Physica D* 215 (2006) 25.
- [39] B. Sandstede, A. Scheel, *Phys. Rev. E* 62 (2000) 7708.
- [40] Y. Hosono, *Bull. Math. Biol.* 60 (1998) 435.
- [41] I.S. Aranson, L. Kramer, *Rev. Modern Phys.* 74 (2002) 99.
- [42] A. Doelman, T.J. Kaper, *SIAM J. Appl. Dyn. Syst.* 2 (2003) 53.
- [43] T. Kolokolnikov, J. Wei, *Appl. Math. Lett.* 18 (2005) 951.
- [44] A. Doelman, B. Sandstede, A. Scheel, G. Schneider, *Mem. Amer. Math. Soc.* (in press).